



Synthesis and spectroscopic investigations of trivalent europium-doped $Z_2Si_3O_8$ ($Z = Mg, Ca$ and Sr) nanophosphors for display applications

Suman Sheoran, Kuldeep Singh, Vijeta Tanwar, Sitender Singh, Anura Samantilleke, Devender Singh*

Received: 25 June 2019/Revised: 14 September 2019/Accepted: 5 March 2020/Published online: 7 April 2020
© The Nonferrous Metals Society of China and Springer-Verlag GmbH Germany, part of Springer Nature 2020

Abstract To explore the silicate lattice-based nanophosphors, a series of Eu^{3+} -doped $Z_2Si_3O_8$ ($Z = Mg, Ca$ and Sr) materials were prepared by sol–gel procedure. The metal nitrates and silica powder were used as precursor components for the synthesis of these luminescent materials. Photoluminescence (PL) emission spectra, powder X-ray diffraction (PXRD), energy-dispersive X-ray spectroscopy (EDS), Fourier transform infrared spectroscopy (FTIR) and transmission electron microscopy (TEM) spectroscopic techniques were applied for the characterization of the fabricated materials. Three peaks were observed at 589, 613 and 650–652 nm corresponding to $^5D_0 \rightarrow ^7F_{1-3}$ transition in PL emission spectra. Upon 395 nm excitation and at 0.03 mol Eu^{3+} , these nanophosphors displayed optimum photoluminescence with the most intense peak analogous to $^5D_0 \rightarrow ^7F_2$ transition of dopant ion. The as-prepared phosphor materials were re-heated at 1050 and 1150 °C to observe the consequences of higher temperatures on the emission intensity and crystal lattice. XRD analysis confirmed that all the synthesized materials were of crystalline nature, and the crystallinity was observed to be improved by increasing the temperature. In the FTIR spectrum, peaks at 483 and 610 cm^{-1} proved the existence of SiO_4 group in $Ca_2Si_3O_8$, and the peak centered at 417 cm^{-1} confirmed the presence of MgO_6 octahedral in $Mg_2Si_3O_8$ materials. TEM images were used to determine the particle size (13–35 nm) and to study the three-

dimensional structure of nanophosphor materials. The experimental studies indicate that these materials may be promising as red-emitting nanophosphors for white light-emitting diodes.

Keywords $Z_2Si_3O_8$; Nanophosphors; Sol–gel; Photoluminescence; Crystalline

1 Introduction

Some recent researches of luminescent materials are paying attention on the improvement of innovative and proficient phosphors with high luminescence efficacy and satisfactory thermal and chemical stability. Silicates and thio-silicate lattice-based phosphor materials have potential applications in the field of lighting, display devices [1, 2], solid-state laser, white light-emitting diodes, luminescent paints, cathode ray tubes, fluorescence and biological labeling and solar panels, etc. [3–5]. The development of phosphors requires appropriate host matrix and suitable metal ion as a dopant. Lanthanide ions have been widely used as activators in different host lattices due to the possibility of various transitions among their abundant energy levels [6, 7]. The higher energy levels of these ions can be populated easily and undergo radiative decay to the ground energy level, resulting in the luminescence. The f-orbitals, deeply embedded in the ions, are protected from the chemical environment and result in sharp emission spectra arising from f–f transitions [8–11]. The red color is one of the prime components for the development of white light-emitting diodes (WLEDs) and displays. The synthesis of red phosphors with satisfactory color rendering index and the suitable emission color performance is crucial for

S. Sheoran, K. Singh, V. Tanwar, S. Singh, D. Singh*
Department of Chemistry, Maharshi Dayanand University,
Rohtak 124001, India
e-mail: devjakhar@gmail.com

A. Samantilleke
Centro de Fisica, Universidade of Minho, Braga 4710057,
Portugal

the development of optoelectronic materials [12–14]. Recent studies have proved Eu^{3+} as the most efficient activator among rare earth ions for the generation of red color [15, 16].

Presently, researchers have synthesized numerous phosphors using abundant experimental techniques including sol–gel [17], hydrothermal [18], microwave, solid-state reaction [19] and solution combustion [20]. The foremost disadvantages of the solid-state method are its long processing time, high reaction temperature, large particle size and luminescence loss due to crushing [21]. In the sol–gel technique, the raw chemicals are blended to get the sol solution with great extent of uniformity; therefore, the addition of dopants and co-dopants through solutions becomes easy and efficient. The gel formed on heating results in the formation of very small pores, and all the ingredients of the uniform gel mix very well. The excessive high surface area of samples is responsible for the low-temperatures synthesis of the materials [22].

In the present study, we have focused on the photoluminescent and structural properties of Eu^{3+} -doped $Z_2Si_3O_8$ ($Z = Mg, Ca$ and Sr) materials. An effective sol–gel procedure has been used to explore these silicate lattice-based materials [23]. To evaluate the intensity and color affluence of these phosphors, the optical properties were examined by the photoluminescence spectroscopy. For structural investigations, the prepared materials were characterized with X-ray diffraction (XRD) analysis, energy-dispersive X-ray spectroscopy (EDS), Fourier transform infrared (FTIR) study and transmission electron microscope (TEM) analysis.

2 Experimental

2.1 Materials and synthesis

The powdered samples of Eu^{3+} -doped $Z_2Si_3O_8$ ($Z = Mg, Ca$ and Sr) phosphors were synthesized by sol–gel process. The nitrates of alkaline earth metals (Mg, Ca and Sr), $Eu(NO_3)_3 \cdot 6H_2O$ and silica powder were used as precursor components for the synthesis of these luminescent materials. Initially, $Sr_2Si_3O_8$ phosphor was prepared using 0.01–0.05 mol europium(III) ion. For optimum photoluminescence performance, the concentration of Eu^{3+} was fixed (i.e., 0.03 mol), and a series of $Z_2Si_3O_8$ silicates were synthesized at 950 °C. The synthetic procedure used to develop silicate lattice-based materials was consisting of two steps. In the first step, 3-mol silica powder was dissolved in a round-bottom flask (RBF) containing concentrated nitric acid solution and stirred using the magnetic stirrer, resulting in the development of smooth gel. Alternatively, alkaline metal nitrates in their stoichiometric amount [$Mg/Ca/Sr$ (1.97 mol)] and $Eu(NO_3)_3 \cdot 6H_2O$

(0.03 mol) were liquefied with distilled water in a silica crucible. The content of crucible was poured into the RBF and stirred up to 30 min for homogeneous mixing. The semisolid paste was formed from the homogeneous mixture when heated in the silica crucible on the hot plate. The crucible that contained semisolid paste was placed in the muffle furnace maintained at the temperature of 950 °C for 1 h, which gave rise to white silicate powders. The influence of heating on the optical properties and crystallinity of materials was investigated by re-heating the samples at the temperatures of 1050 and 1150 °C.

2.2 Characterization

For spectroscopic investigations, all the samples were ground in the agate motor to obtain the powder form, and the examinations were performed at room temperature. The optical characteristics of the prepared materials were measured using a xenon lamp (excitation source)-assisted Horiba Jobin–YVON Fluorolog spectrophotometer. The photoluminescence (PL) emission spectra of the samples were recorded in 400–700 nm regions. The diffraction studies were made with X-ray diffractometer (XRD, Rigaku Ultima IV) using $Cu K\alpha$ radiations (wavelength of 0.15416 nm). XRD patterns of the materials were recorded from 15° to 70° (2θ) at 4 (°)·min⁻¹, scanning speed of 4 (°)·min⁻¹ and step interval of 0.02°. Energy-dispersive X-ray fluorescence spectrometer (Panalytical Epsilon 5) was used for the elemental analysis in these phosphor materials. TEM (TECNAI, 200 kV, Fei. Electron Optics) was used to evaluate the particle size of the fabricated silicate phosphors. The chemical environment and arrangement of different elements inside luminescent materials were analyzed from FTIR spectra collected using Bruker Alpha FTIR spectrophotometer.

3 Results and discussions

3.1 Fluorescence characterization

The PL emission spectra of these materials show sharp spectral lines from 400 to 700 nm due to the presence of Eu^{3+} . The characteristics red emission of the as-prepared samples under ultraviolet excitation in the UV lamp is shown in Fig. 1. The optical emissions of the synthesized materials were recorded at 395 nm excitation. Figure 2 displays the graphical representation of synthetic route used for the fabrication of focused phosphors. The luminescence power of prepared phosphors was found to increase without any change in the spectral shape upon increase in Eu^{3+} concentration. However, the photoluminescent quenching starts as the concentration exceeds

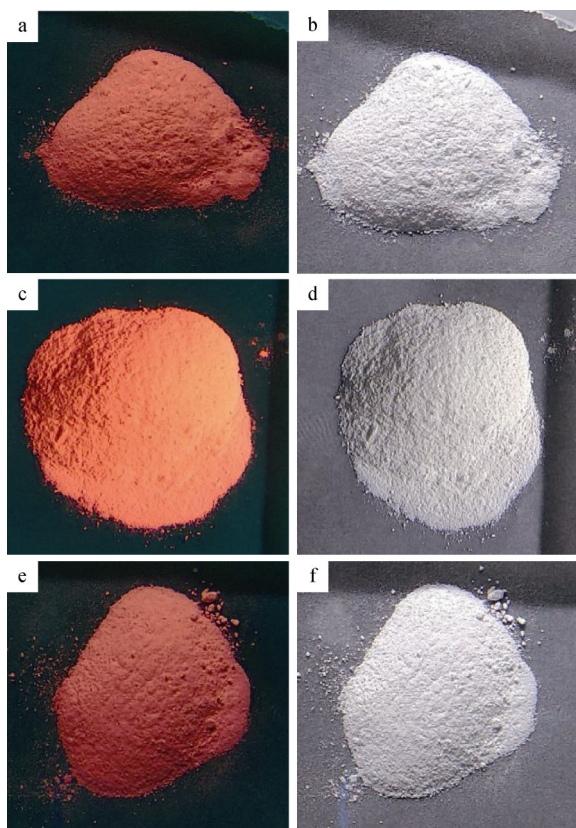


Fig. 1 Macro-images of phosphors by stimulating them in UV light and the absence of UV light: **a, b** $\text{Mg}_2\text{Si}_3\text{O}_8:\text{Eu}^{3+}$, **c, d** $\text{Ca}_2\text{Si}_3\text{O}_8:\text{Eu}^{3+}$ and **e, f** $\text{Sr}_2\text{Si}_3\text{O}_8:\text{Eu}^{3+}$

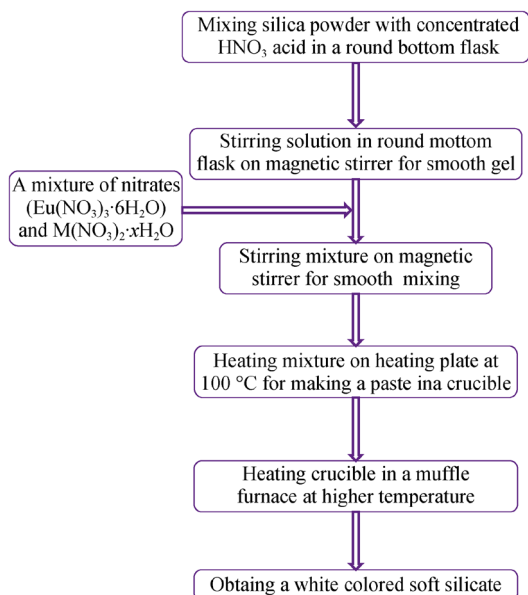


Fig. 2 Graphical representation displaying synthetic route of silicate phosphor

0.03 mol. The increased amount of dopants in the lattice results in an enhanced non-radiative decay, consequently, radiative emission and luminous intensity decrease [24]. The most effective Eu^{3+} concentration in the present matrix is 0.03 mol. Hence, the photoluminescence characteristics are sensitive to the composition of activator ion in the crystal matrix. Figure 3 shows typical PL emission spectra of $\text{Sr}_2\text{Si}_3\text{O}_8$ with europium ion concentration of 0.01–0.05 mol.

Figure 4 depicts the fluorescence spectra of $\text{Z}_2\text{Si}_3\text{O}_8$ materials recorded at 395 nm excitation. The emission spectra exhibits three peaks which can be ascribed to $^5\text{D}_0 \rightarrow ^7\text{F}_{1-3}$ transitions, and these spectral peaks confirm the availability of europium(III) ion in crystal lattice. Out of these, $^5\text{D}_0 \rightarrow ^7\text{F}_1$ and $^5\text{D}_0 \rightarrow ^7\text{F}_2$ are magnetic- and electric-dipole-allowed transitions correspondingly. The electric-dipole allowed transition is more intense compared to the magnetic dipole transition due to lack of inversion symmetry around europium(III) ions [25, 26]. The higher value of intensity ratio indicates the greater asymmetry around Eu^{3+} ions in the crystal lattice. The highest photoluminescence emission is observed in Eu^{3+} -doped $\text{Mg}_2\text{Si}_3\text{O}_8$ phosphor as shown in Fig. 5. The peak positions and colors corresponding to these prepared materials are given in Table 1.

The effect of the change in temperature on the luminescence strength was also studied by recording the emission spectra of samples re-heated at higher temperatures of 1050 and 1150 °C. The emission intensity has been observed to increase without any change of the spectral shape upon the increase in temperature for respective phosphors. The increase in luminous intensity with rise in the temperature is the result of the increase in radiative phenomenon at a higher temperature. It is worthwhile to point out that the prepared materials display excellent photoluminescence and thermo-stability, even at higher temperatures [27].

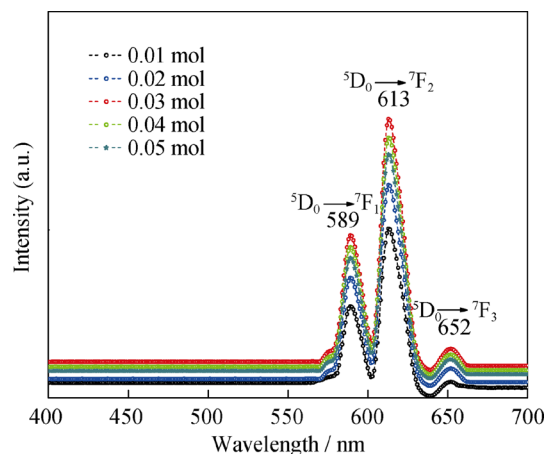


Fig. 3 Fluorescent intensity with concentration of Eu^{3+} doped in $\text{Sr}_2\text{Si}_3\text{O}_8$ phosphor

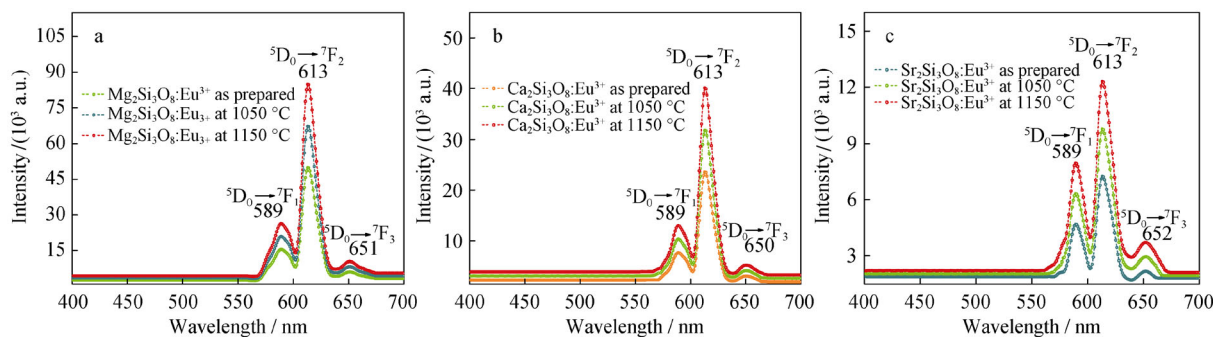


Fig. 4 Photoluminescence emission spectra of Eu³⁺-activated Z₂Si₃O₈ phosphors: **a** Mg₂Si₃O₈, **b** Ca₂Si₃O₈ and **c** Sr₂Si₃O₈

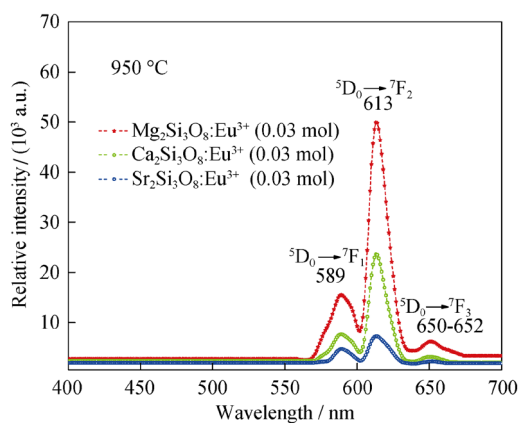


Fig. 5 Relative PL emission spectra of Eu³⁺-activated Z₂Si₃O₈ (Z = Mg, Ca and Sr) fluorescent materials

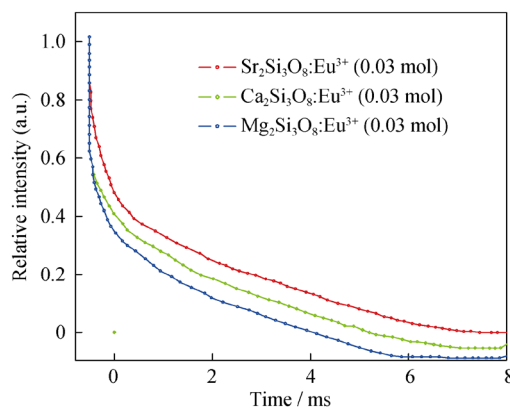


Fig. 6 Decay profiles of Eu³⁺-doped phosphor materials at 950 °C

3.2 Decay spectra of phosphors

Figure 6 depicts the decay behavior of Eu³⁺-doped phosphor materials explored at 950 °C for the emission of ⁵D₀ → ⁷F₂ transition. Decay time resulting from single exponential function is well-fitted according to Eq. (1):

$$I(t) = I_0 \exp(-t/\tau) \tag{1}$$

where *I*(*t*) and *I*₀ represent the luminescence intensity at time *t* and 0, respectively, and τ is the decay time of the phosphor materials. Table 2 summarizes the decay time values of the Eu³⁺-doped phosphor materials.

The Commission International de l’Eclairage (CIE) color coordinates values are very important considerations to determine the emissive region for inorganic phosphors.

Table 2 CIE color coordinates and decay time values of Eu³⁺-activated silicates nanophosphors at respective temperatures

Materials	950 °C		1050 °C		1150 °C		Decay time/ms (950 °C)
	x	y	x	y	x	y	
Mg ₂ Si ₃ O ₈ :Eu ³⁺	0.53	0.35	0.54	0.35	0.55	0.35	1.23
Ca ₂ Si ₃ O ₈ :Eu ³⁺	0.47	0.34	0.48	0.34	0.49	0.34	1.37
Sr ₂ Si ₃ O ₈ :Eu ³⁺	0.40	0.34	0.42	0.34	0.44	0.34	1.96

Table 2 shows the color coordinates value calculated by CIE calculator for the respective phosphors at different temperatures. Figure 7 depicts the CIE triangle, showing that the samples emit pure reddish light, which supports the PL analysis of the present phosphors [28].

Table 1 Various transitions, main peak and color of Eu³⁺-activated silicates materials

Materials	⁵ D ₀ → ⁷ F ₁ /nm	⁵ D ₀ → ⁷ F ₂ /nm	⁵ D ₀ → ⁷ F ₃ /nm	Main peak/nm	Color
Mg ₂ Si ₃ O ₈ :Eu ³⁺	589	613	651	613	Red
Ca ₂ Si ₃ O ₈ :Eu ³⁺	589	613	650	613	Red
Sr ₂ Si ₃ O ₈ :Eu ³⁺	589	613	652	613	Orange red

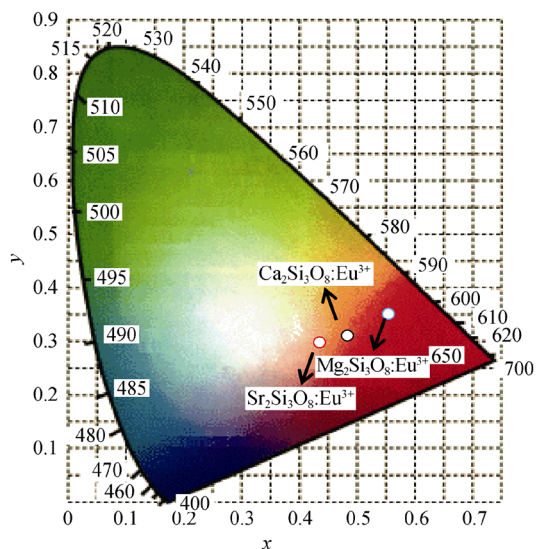


Fig. 7 Color triangle demonstrating CIE coordinates synthesized phosphors at 1150 °C

3.3 PXRD measurements

PXRD patterns of sol–gel-derived $Z_2Si_3O_8$ phosphors are shown in Fig. 8. Eu^{3+} -doped $Z_2Si_3O_8$ materials show peaks in 15° – 70° region, reflecting the highly crystalline nature of these phosphors. The diffraction peaks for Eu^{3+} -doped $Mg_2Si_3O_8$ phosphor are available at 2θ of 17.19° , 22.87° , 23.87° , 25.43° , 27.99° , 29.84° , 30.98° , 32.26° , 39.79° , 41.78° , 52.30° , 61.97° and 62.82° . The main intense peaks for this phosphor are found at 35.68° and 36.52° . There is no pre-literature available to confirm the crystal structure of the synthesized phosphors. Literature study is available only for $Ba_2Si_3O_8$ materials with application in light-emitting diodes (LEDs) development [29, 30].

$Ca_2Si_3O_8$ phosphor shows diffraction peaks at 2θ of 25.43° , 27.71° , 29.84° , 31.83° , 36.09° , 38.3° , 41.35° , 45.76° , 49.60° , 53.30° , 56.70° , 57.10° , 60.10° and 62.96° with the most intense peak at 21.72° . At a temperature of $1150^\circ C$, these materials exist in the same crystalline form

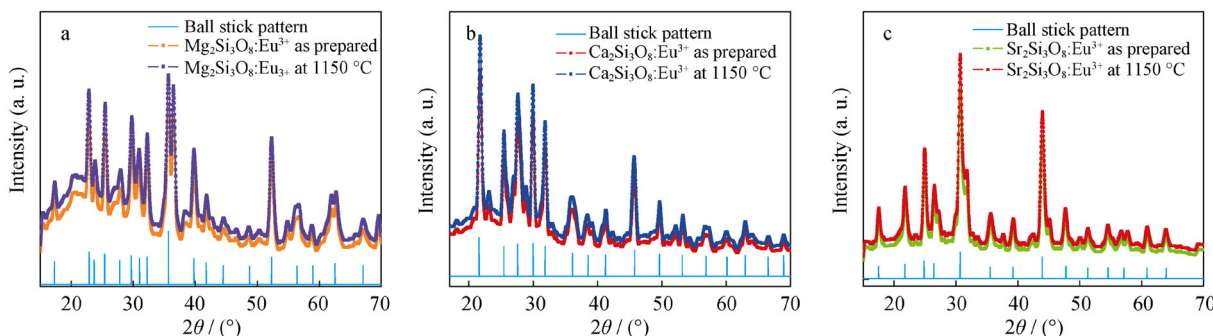


Fig. 8 XRD patterns of $Z_2Si_3O_8:Eu^{3+}$ samples: **a** $Mg_2Si_3O_8:Eu^{3+}$, **b** $Ca_2Si_3O_8:Eu^{3+}$ and **c** $Sr_2Si_3O_8:Eu^{3+}$

as at $950^\circ C$, and the increase in temperature enhances the particle size of the phosphor materials. The diffraction pattern of these phosphors does not match with that of their corresponding Z_2SiO_4 - and $ZSiO_3$ -based phosphors, indicating that there would be the complete formation of $Z_2Si_3O_8$ ($Z = Mg, Ca$ and Sr) phosphors. Although charge and size issues exist where substitution of Z^{2+} (Mg^{2+} , Ca^{2+} and Sr^{2+}) in the lattice occurs by Eu^{3+} , each time there will be a different diffraction pattern observed for these materials. It means these exist in a different crystalline form. The crystallinity and intensity of peak enhance by increasing the temperature of these phosphors as shown in Fig. 8. $Sr_2Si_3O_8$ silicate shows peaks at 17.47° , 21.74° , 25.00° , 26.43° , 35.66° , 39.22° , 43.92° , 47.75° , 56.70° and 57.85° ; however, most intense XRD peaks are present at 30.68° and 31.68° . The crystallite size calculations were performed by applying Debye–Scherrer's formula.

$$D = 0.9\lambda / \beta \cos \theta \quad (2)$$

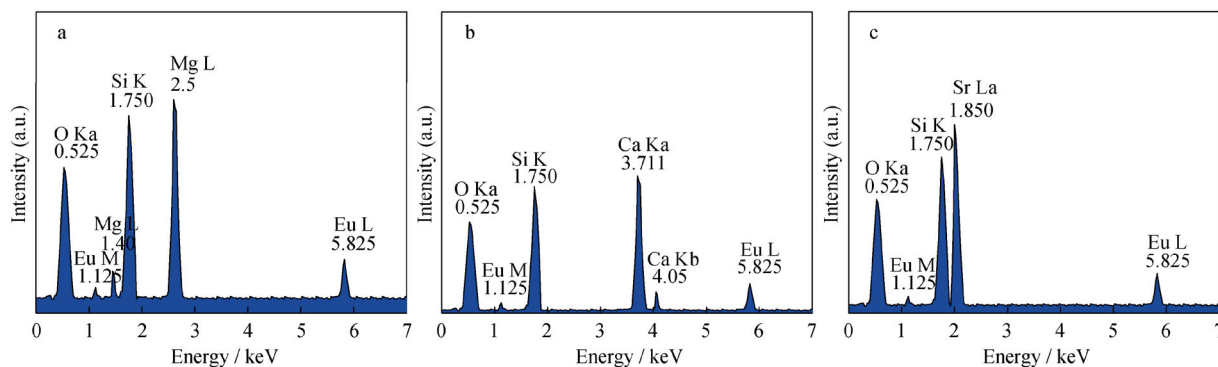
where D is crystallite size, k is a constant (0.89), β denotes full width at half maximum, λ is the wavelength of X-ray, and θ stands for incident Bragg's angle. The crystallite size and crystallinity of the materials strongly influence the luminescence intensity. The particle sizes of synthesized phosphors particles are shown in Table 3.

3.4 EDS analysis

Figure 9 represents EDS profiles of the sol–gel-derived $Z_2Si_3O_8$ phosphor materials. The spectra demonstrate large number of peaks that belong to different elements incorporated within the host frame. The peaks accessible at 0.525 keV (O), 1.750 keV (Si), 1.125 and 5.825 keV (Eu), 1.400 and 2.500 keV (Mg), 3.711 and 4.050 keV (Ca) and 1.850 keV (Sr) approve the existence of these elements in the frame. The occurrence of Eu^{3+} peaks in the spectra reveals the consistent mixing of ions in the silicate lattice. Nonexistence of other peaks designates the pure formation of $Z_2Si_3O_8$ phosphor materials. Table 4 signifies the

Table 3 Different characteristics of XRD analysis of $Z_2Si_3O_8$ ($Z = Mg, Ca$ and Sr) materials

Type of phosphor	$2\theta/(\circ)$	Area	Width/ (\circ)	FWHM/rad	Crystallite size/nm
$Mg_2Si_3O_8:Eu^{3+}$	35.68	27057.786	1.6730	0.01460	11.70
$Ca_2Si_3O_8:Eu^{3+}$	21.72	21262.267	0.7030	0.00600	24.34
$Sr_2Si_3O_8:Eu^{3+}$	30.68	43983.709	0.7603	0.00663	28.21


Fig. 9 EDS spectra of Eu^{3+} -doped $Z_2Si_3O_8$ phosphor materials calcined at $950\text{ }^\circ\text{C}$: **a** $Mg_2Si_3O_8:Eu^{3+}$, **b** $Ca_2Si_3O_8:Eu^{3+}$ and **c** $Sr_2Si_3O_8:Eu^{3+}$

compositions of the explored materials, which are in good consistency with the stoichiometric ratio of precursors used for their formation.

3.5 FTIR spectroscopy

The chemical structure of Eu^{3+} -doped $Z_2Si_3O_8$ phosphors was analyzed by recording FTIR spectra, as shown in Fig. 10. The sharp peaks at 483 and 610 cm^{-1} prove the presence of SiO_4 group in the spectra of $Ca_2Si_3O_8$ phosphor [31, 32]. In the FTIR spectrum of $Mg_2Si_3O_8$ phosphor, the peak present at 417 cm^{-1} is due to the MgO_6 octahedral [33, 34]. The peaks located in between 400 and 1300 cm^{-1} region give rise to bands due to stretching and bending modes of silicate bonds. Appearance of peak at 417 cm^{-1} in $Ca_2Si_3O_8$ phosphor is due to the lattice vibrations of $Ca-O$ bond. Peaks centered at 675 and 679 cm^{-1} in the FTIR spectra of $Mg_2Si_3O_8$ and $Ca_2Si_3O_8$ materials are due to the $Si-O$ bond. The band for stretching vibration of $Sr-O$ bond is reported around 1481 cm^{-1} ;

however, corresponding peak is located at 1470 cm^{-1} in $Sr_2Si_3O_8$ phosphor.

3.6 TEM study

TEM is a powerful tool to evaluate the crystallite size of synthesized phosphor materials. The morphological studies including the studies of shape and size of particles were investigated via TEM analysis. Figure 11 displays TEM images of europium(III)-doped $Z_2Si_3O_8$ ($M = Mg, Ca$ and Sr) phosphor materials. All the $Z_2Si_3O_8$ consist of nanoparticles which aggregate with nearly spherical morphology. The unbalanced distribution of the flow of mass and temperature during the synthesis of material is responsible for the abnormality in the shape and size of particles. The particle size of the prepared materials lies in $13\text{--}35\text{ nm}$ range, and this nano-granular size is clearly observed in their TEM micrographs. The particle size as estimated from these micrographs has been found in accordance with the size calculated from XRD investigations. The nano-range particles have made them suitable for various advanced display technologies and lighting purposes. Table 5 shows the particle sizes of the samples investigated via TEM analysis and Scherer's equation.

Table 4 Compositions of phosphor materials from EDX analysis

Materials	w/wt%			x/at%		
	(Mg, Ca and Sr)	Eu^{3+}	Si	(Mg, Ca and Sr)	Eu^{3+}	Si
$Mg_2Si_3O_8:Eu^{3+}$	82.80	3.01	14.19	78.40	3.28	18.32
$Ca_2Si_3O_8:Eu^{3+}$	76.02	3.23	20.75	77.87	3.04	19.09
$Sr_2Si_3O_8:Eu^{3+}$	73.40	3.12	23.48	72.98	3.34	23.68

4 Conclusion

Novel silicate $Z_2Si_3O_8$ ($Z = Mg, Ca$ and Sr) materials were prepared by simple, effectual and rapid sol-gel process at the temperature of $950\text{ }^\circ\text{C}$. These samples were further

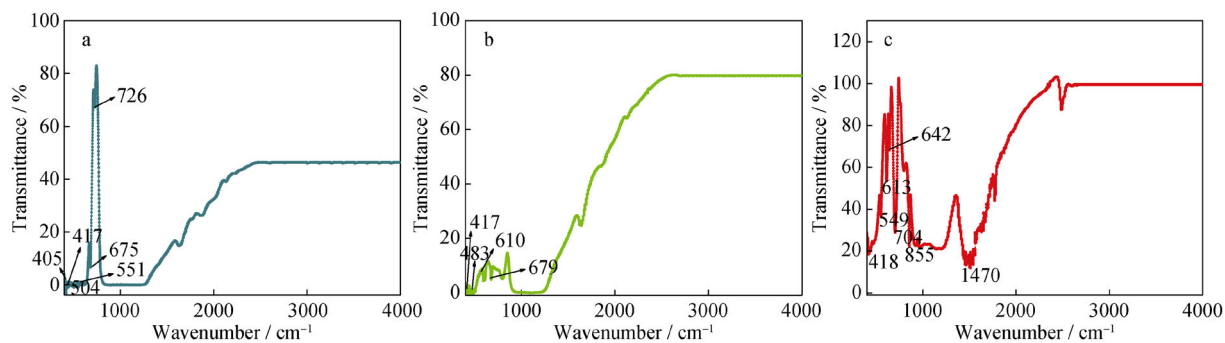


Fig. 10 FTIR spectra of Eu^{3+} -doped $\text{Z}_2\text{Si}_3\text{O}_8$ phosphors calcined at 950°C : **a** $\text{Mg}_2\text{Si}_3\text{O}_8:\text{Eu}^{3+}$, **b** $\text{Ca}_2\text{Si}_3\text{O}_8:\text{Eu}^{3+}$ and **c** $\text{Sr}_2\text{Si}_3\text{O}_8:\text{Eu}^{3+}$

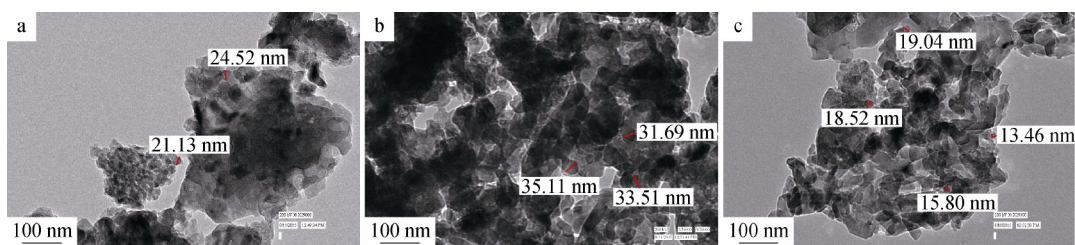


Fig. 11 TEM images of fluorescent materials calcined at 950°C : **a** $\text{Mg}_2\text{Si}_3\text{O}_8:\text{Eu}^{3+}$, **b** $\text{Ca}_2\text{Si}_3\text{O}_8:\text{Eu}^{3+}$ and **c** $\text{Sr}_2\text{Si}_3\text{O}_8:\text{Eu}^{3+}$

Table 5 Particle size values investigated from diffraction data and TEM (nm)

Measured methods	$\text{Mg}_2\text{Si}_3\text{O}_8:\text{Eu}^{3+}$	$\text{Ca}_2\text{Si}_3\text{O}_8:\text{Eu}^{3+}$	$\text{Sr}_2\text{Si}_3\text{O}_8:\text{Eu}^{3+}$
TEM	21.13	33.51	19.02
XRD	11.70	24.45	28.81

calcined at the temperatures of 1050 and 1150°C to examine the influence of temperature on the luminescence intensity and crystallinity of the materials. The luminescent properties of the samples were studied by recording their emission spectra under the excitation of 395 nm . The PL emission spectra show that these phosphors after re-heating at 1150°C and at 0.03 mol Eu^{3+} exhibit maximum luminescence intensity. Three characteristic emission bands were obtained at 589 , 613 and $650\text{--}652\text{ nm}$ which were accredited to ${}^5\text{D}_0 \rightarrow {}^7\text{F}_{1-3}$ transitions. The dominant peak at 613 nm (${}^5\text{D}_0 \rightarrow {}^7\text{F}_2$) is responsible for the red color of these materials. The PL investigation confirms that these phosphors show excellent color stability. The CIE color coordinates values of phosphor lie in the red region, confirming the PL results. PXRD patterns have shown highly sharp and intense peaks in $15^\circ\text{--}70^\circ$ region. FTIR spectra confirm the presence of SiO_4 group and MgO_6 octahedral in the $\text{Ca}_2\text{Si}_3\text{O}_8$ and $\text{Mg}_2\text{Si}_3\text{O}_8$ phosphor, respectively. The chemical structure of the prepared silicates analyzed

through FTIR analysis is found in good agreement with XRD analysis. TEM results appeared reliable with PXRD examinations. The brilliant photoluminescence intensity of as-prepared samples reveals that the focused phosphors could have potential applications in WLEDs, scintillators, fluorescent panels and display technologies.

References

- [1] Lee SP, Chan TS, Chen TM. Novel reddish-orange-emitting $\text{BaLa}_2\text{Si}_2\text{S}_8:\text{Eu}^{2+}$ thiosilicate phosphor for LED lighting. *ACS Appl Mater Interfaces*. 2015;7(1):40.
- [2] Tian B, Chen B, Tian Y, Li X, Zhang J, Sun J, Zhong H, Cheng L, Fu S, Zhong H, Wang Y, Zhang X, Xia H, Hua R. Excitation pathway and temperature dependent luminescence in color tunable $\text{Ba}_5\text{Gd}_8\text{Zn}_4\text{O}_{21}:\text{Eu}^{3+}$ phosphors. *J Mater Chem C*. 2013; 1(12):2338.
- [3] Tian Y, Chen B, Hua R, Sun J, Cheng L, Zhong H, Li X, Zhang J, Zheng Y, Yu T, Huang L, Yu H. Optical transition, electron-phonon coupling and fluorescent quenching of $\text{La}_2(\text{MoO}_4)_3:\text{Eu}^{3+}$ phosphor. *J Appl Phys*. 2011;109(5):053511.
- [4] Singh V, Rai VK, Al-Shamerya K, Nordmann J, Haase M. NIR to visible in $\text{Er}^{3+}/\text{Yb}^{3+}$ co-doped CaYAl_3O_7 phosphor obtained by solution combustion process. *J Lumin*. 2011;131(12):2679.
- [5] Chang C, Li W, Huang X, Wang Z, Chen X, Qian X, Guo R, Ding Y, Mao D. Photoluminescence and afterglow behavior of Eu^{2+} , Dy^{3+} and Eu^{3+} , Dy^{3+} in $\text{Sr}_3\text{Al}_2\text{O}_6$ matrix. *J Lumin*. 2010; 130(3):347.
- [6] Dutta DP, Tyagi AK. Inorganic phosphor materials for solid state white light generation. *Solid State Phenom*. 2009;155:113.
- [7] Singh D, Tanwar V, Simantilke AP, Mari B, Kadyan PS, Singh I. Rapid synthesis and photoluminescent characterization of $\text{MAl}_2\text{O}_4:\text{Eu}^{2+}$, Dy^{3+} ($\text{M} = \text{Ca}/\text{Ca} + \text{Ba}/\text{Ca} + \text{Mg}$) blue

- nanophosphors for white lighting display applications. *Adv Mater Lett.* 2016;7(1):47.
- [8] Liu B, Ding D, Liu Z, Chen F, Xia C. Synthesis and electrical conductivity of various melilite-type electrolytes $Ln_{1+x}Sr_{1-x}Ga_3O_{7+x/2}$. *Solid State Ion.* 2011;191(1):68.
- [9] Yu H, Yu X, Xu X, Jiang T, Yang P, Jiao Q, Zhou D, Qiu J. Excitation band extended in $CaYAl_3O_7:Tb^{3+}$ phosphor by Ce^{3+} co-doped for NUV light-emitting diodes. *Opt Commun.* 2014;317:78.
- [10] Mahakhode JG, Dhoble SJ, Joshi CP, Moharil SV. Combustion synthesis of phosphor for plasma display panels. *J Alloy Compd.* 2007;438(1–2):293.
- [11] Mo F, Zhou L, Pang Q, Lan Y, Liang Z. Synthesis and luminescent properties of $Zn_{0.890}Nb_2O_6:Eu_{0.05}^{3+}, Bi_{0.005}^{3+}, M_{0.055}^{+}$ (M = Li, Na, K) phosphors. *Curr Appl Phys.* 2013;13(2):331.
- [12] Bandi VR, Nien YT, Lu TH, Chen IG. Effect of calcination and concentration on luminescence properties of Novel $Ca_3Y_2Si_3O_{12}:Eu$ phosphor. *J Am Ceram Soc.* 2009;92(12):2953.
- [13] Kadukar MR, Yawalkar PW, Choithrani R, Dhoble SJ. Mechanoluminescence, thermoluminescence, photoluminescence studies on $Ca_3Y_2Si_3O_{12}:RE^{3+}$ ($RE^{3+} = Dy^{3+}$ and Eu^{3+}) phosphors. *J BioluminChemilumin.* 2015;30(8):1219.
- [14] Park JK, Choi KJ, Kang HG, Kim JM, Kim CH. Silicates phosphors for white LEDs identified through combinatorial chemistry. *Electrochem Solid-State Lett.* 2007;10(2):J15.
- [15] Thakur J, Dutta DP, Bagla H, Tyagi AK. Effect of host structure and concentration on the luminescence of Eu^{3+} and Tb^{3+} in borate phosphors. *J Am Ceram Soc.* 2012;95(2):696.
- [16] Dutta DP, Roy M, Tyagi AK. Dual function of rare earth doped nano Bi_2O_3 : white light emission and photocatalytic properties. *Dalton Trans.* 2012;41(34):10238.
- [17] Singh D, Sheoran S, Singh J. Optical characterization of Eu^{3+} doped $MLSiO_4$ (M = Ca, Sr, Ba and L = Mg) phosphor materials for display devices. *J Mater Sci: Mater Electron.* 2018;29(1):294.
- [18] Kumada N, Yanagida S, Takei T, Hong B. Hydrothermal synthesis and crystal structure of new red phosphors, $KNaMF_7:Mn^{4+}$ (M: Nb, Ta). *Mater Res Bull.* 2019;115:170.
- [19] Chen Y, Wang M, Wang J, Wu M, Wang C. A high color purity red emitting phosphor $CaYAIO_4:Mn^{4+}$ for LEDs. *J Solid State Light.* 2014;1:15.
- [20] Singh D, Kadyan S. Synthesis and optical characterization of trivalent europium doped $M_4Al_2O_9$ (M = Y, Gd and La) nanomaterials for display applications. *J Mater Sci: Mater Electron.* 2017;28(15):11142.
- [21] Singh D, Tanwar V, Samantilleke AP, Mari B, Bhagwan S, Singh KC, Kadyan PS, Singh I. Synthesis of $Sr_{(1-x-y)}Al_4O_7:Eu_x^{2+}, Ln_y^{3+}$ (Ln = Dy, Y, Pr) nanophosphors using rapid gel combustion process and their down conversion characteristics. *Electron Mater Lett.* 2017;13(3):222.
- [22] Rao RP. Preparation and characterization of fine-grain yttrium-based phosphors by sol–gel process. *J Electrochem Soc.* 1996;143(1):189.
- [23] Singh D, Sheoran S. Synthesis and luminescent characteristics of $M_3Y_2Si_3O_{12}:Eu^{3+}$ (M = Ca, Mg, Sr and Ba) nanomaterials for display applications. *J Mater Sci: Mater Electron.* 2016;27(12):12707.
- [24] Singh D, Kadyan S, Bhagwan S. Structural and photoluminescence characteristics of $M_3Al_5O_{12}:Eu^{3+}$ (M = Y, Gd and La) nanophosphors for optoelectronic applications. *J Mater Sci: Mater Electron.* 2017;28(18):13478.
- [25] Hertle E, Chepyga L, Batentschuk M, Zigan L. Influence of codoping on the luminescence properties of YAG: Dy for high temperature phosphor thermometry. *J Lumin.* 2017;182:200.
- [26] Matos MG, Pereira PFS, Calefi PS, Ciuffi KJ, Nassar EJ. Preparation of a $GdCaAl_3O_7$ matrix by the non-hydrolytic sol–gel route. *J Lumin.* 2009;129(10):1120.
- [27] Singh J, Baitha PK, Manam J. Influence of heat treatment on the structural and optical properties of $SrGd_2O_4:Eu^{3+}$ phosphor. *J Rare Earths.* 2015;33(10):1040.
- [28] Sahu IP, Bisen DP, Brahme N, Tamrakar RK, Shrivastava R. Luminescence studies of dysprosium doped strontium aluminate white light emitting phosphor by combustion route. *J Mater Sci: Mater Electron.* 2015;26(11):8824.
- [29] Xiao F, Xue YN, Zhang QY. Bluish-green color emitting $Ba_2Si_3O_8:Eu^{2+}$ ceramic phosphors for white light-emitting diodes. *Spectrochim Acta A Mol Biomol Spectrosc.* 2009;74(3):758.
- [30] Chen M, Xia Z, Molokeev MS, Liu Q. Insights into $Ba_4Si_6O_{16}$ structure and photoluminescence tuning of $Ba_4Si_6O_{16}:Ce^{3+}, Eu^{2+}$ phosphors. *J Mater Chem C.* 2015;3:12477.
- [31] Shrivastava R, Kaur J, Chandra BP. Mechanoluminescence of $Ba_2MgSi_2O_7$ doped with Eu^{2+} and Dy^{3+} phosphor by impulsive deformation. *J BioluminChemilumin.* 2015;30(8):1207.
- [32] Fang YC, Kao PC, Yang YC, Chu SY. Two-Step Synthesis of $SrSi_2O_2N_2:Eu^{2+}$ Green oxynitride phosphor: electron-phonon coupling and thermal quenching behavior. *J Electrochem Soc.* 2011;158(8):J246.
- [33] Naik R, Prashantha SC, Nagabhushana H, Sharma SC, Nagaswarupa HP, Anantharaju KS, Nagabhushana BM, Premkumar HB, Girish KM. A single phase, red emissive $Mg_2SiO_4:Sm^{3+}$ nanophosphor prepared via rapid propellant combustion route. *Spectrochim Acta Part A Mol Biomol Spectrosc.* 2015;140:516.
- [34] Mondal K, Kumari P, Manam J. Influence of doping and annealing temperature on the structural and optical properties of $Mg_2SiO_4:Eu^{3+}$ synthesized by combustion method. *Curr Appl Phys.* 2016;16(7):707.